Pushing the boundaries of chemistry? It takes #HumanChemistry

Make your curiosity and talent as a chemist matter to the world with a specialty chemicals leader. Together, we combine cutting-edge science with engineering expertise to create solutions that answer real-world problems. Find out how our approach to technology creates more opportunities for growth, and see what chemistry can do for you at:

evonik.com/career

EVONIK
Leading Beyond Chemistry

Engineering DNA-Grafted Quatsomes as Stable Nucleic Acid-Responsive Fluorescent Nanovesicles

Marianna Rossetti, Lorenzo Stella, Judit Morlà-Folch, Sara Bobone, Ariadna Boloix, Lorena Baranda, Danila Moscone, Mònica Roldán, Jaume Veciana, Miguel F. Segura, Mariana Köber,* Nora Ventosa,* and Alessandro Porchetta*

The development of artificial vesicles into responsive architectures capable of sensing the biological environment and simultaneously signaling the presence of a specific target molecule is a key challenge in a range of biomedical applications from drug delivery to diagnostic tools. Herein, the rational design of biomimetic DNA-grafted quatsome (QS) nanovesicles capable of translating the binding of a target molecule to amphiphilic DNA probes into an optical output is presented. QSs are synthetic lipid-based nanovesicles able to confine multiple organic dyes at the nanoscale, resulting in ultra-bright soft materials with attractiveness for sensing applications. Dye-loaded QS nanovesicles of different composition and surface charge are grafted with fluorescent amphiphilic nucleic acid-based probes to produce programmable FRET-active nanovesicles that operate as highly sensitive signal transducers. The photophysical properties of the DNA-grafted nanovesicles are characterized and the highly selective, ratiometric detection of clinically relevant microRNAs with sensitivity in the low nanomolar range are demonstrated. The potential applications of responsive QS nanovesicles for biosensing applications but also as functional nanodevices for targeted biomedical applications is envisaged.

1. Introduction

The responsive surface recognition properties of biological membranes have inspired a number of strategies for the design and manufacturing of biomimetic artificial vesicles. Synthetic vesicles are self-assembled colloidal particles composed of amphiphilic molecules enclosing a small aqueous compartment.[1–3] Such bilayer structures can be composed of natural or synthetic amphiphilic molecules ranging from lipids to surfactants and block copolymers.[4] Among these, lipid-based nanoparticles bear the advantage of being the least toxic for in vivo applications.[5] To sense and respond to their external environment, integration of specific binding sites within the vesicle structure or post-synthesis functionalization of the external layer with amphiphilic molecular probes have represented the main strategies so far.

Anchoring amphiphilic nucleic acid probes to lipid-based vesicles has found wide application in the production of new biomimetic hybrid structures like DNA-grafted liposomes,[6–8] artificial organelles,[9] and membrane pores.[10–12] Thanks to the selectivity and programmability of Watson-Crick base-pairing interactions, the embedding of synthetic DNA amphiphiles into artificial vesicles allowed the production of DNA-programmed functional materials[13,14] with applications in bottom-up synthetic biology[15–17] and drug delivery.[18,19] In this regard, recently, supramolecular organization of multiple lipid-based vesicles mediated by nucleic

M. Rossetti, L. Stella, S. Bobone, L. Baranda, D. Moscone, A. Porchetta
Department of Chemical Science and Technologies
University of Rome Tor Vergata
Via della Ricerca Scientifica, Rome 00133, Italy
E-mail: alessandro.porchetta@uniroma2.it

J. Morlà-Folch, J. Veciana, M. Köber, N. Ventosa
Institut de Ciència de Materials de Barcelona
ICMAB-CSIC
Campus UAB, Bellaterra 08193, Spain
E-mail: mkober@icmab.es; ventosa@icmab.es

The ORCID identification number(s) for the author(s) of this article can be found under https://doi.org/10.1002/adfm.202103511.

A. Boloix, M. F. Segura
Laboratory of Translational Research in Childhood and Adolescent Cancer
Vall d'Hebron Research Institute (VHIR)-UAB
Barcelona 08035, Spain

M. Roldán
Unitat de Microscòpia Confocal i Imatge Cellular
Servei de Medicina Genètica i Molecular
Institut Pediàtric de Malalties Rares (IPER)
Hospital Sant Joan de Déu
Esplugues de Llobregat, Barcelona 08950, Spain

M. Roldán
Institut de Recerca Sant Joan de Déu
Esplugues de Llobregat, Barcelona 08950, Spain

J. Veciana, M. Köber, N. Ventosa
Centro de Investigación Biomédica en Red CIBER-BBN
Madrid 28029, Spain

J. Veciana, N. Ventosa
Nanomol Technologies SL
Mòdul de Recerca B
Campus Universitari de Bellaterra
Cerdanyola del Vallès 08950, Spain
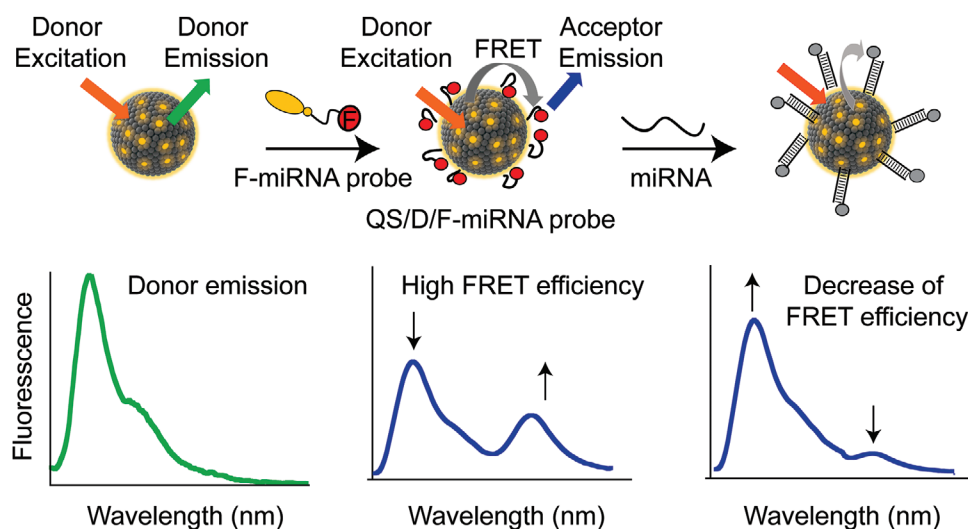
Scheme 1. Schematic representation of the DNA-grafted QS nanovesicles. QSs loaded with an organic fluorophore (i.e., donor) are prepared, and a fluorescent 5′-end cholesteryl-triethylene glycol (TEG) modified DNA probe (i.e., F-miRNA probe) is added to the colloidal system in order to self-assemble into the membrane. The incorporation of the fluorescent amphiphilic DNA probe within the nanovesicle membrane results in FRET between embedded donors (D) and acceptors on the probe (F). In the presence of the specific target miRNA, the hybridization event produces a single- to double strand conformational change of the DNA probe, resulting in a decreased FRET efficiency due to the average distance increase between FRET donor and acceptor.

acid interactions has been reported.[20,21] Such structures can be held together by nucleic acid linkers in order to achieve fusion of multiple vesicle populations[22] and construct compartmentalized chemical processes,[23] and they can be used to study the physical properties of lipid-based self-assembled systems.[7,24]

Several efforts have been devoted to engineer vesicles responsive to physical or molecular stimuli.[25–27] In this regard, aggregation and fusion of lipid vesicles represent two dynamic processes that can be regulated by target binding to recognition elements anchored on the vesicle surface. These phenomena generally produce morphological changes of vesicles and transduce molecular recognition into detectable responses (e.g., changes in light scattering or sample turbidity). Unfortunately, the morphology of self-assembled soft phases can be strongly affected by small changes in the adhesion forces that are generally independent from the nature of the ligand.[28] As a consequence, environmental changes can hamper the applicability of the vesicular systems for sensing applications.

Quatsomes (QSs) are an emerging class of highly stable small unilamellar vesicles of ≈50–100 nm in diameter, formed by the self-assembly of ionic surfactants and sterols in aqueous media.[29,30] Their high stability, that is, also in body fluids,[31] unilamellarity and particle-to-particle homogeneity make them an attractive soft material for sensing applications. Furthermore, we recently demonstrated the possibility to confine hundreds of organic dyes in a single QS[32–34] and even the simultaneous loading of a Förster resonance energy transfer (FRET) dye pair in QSs yielding ultra-bright nanovesicles, whose brightness compares with the most common quantum dots,[35] enabling their use for molecular detection and imaging. Finally, the cellular penetration capability of different types of fluorescent QSs in different cell lines has been also reported.[32–35] In this respect, introducing responsiveness to external molecular inputs within fluorescent QS nanovesicle could pave the way for the rational design of multifunctional biomimetic vesicles

capable of translating the recognition of target molecules into signal transduction for biosensing applications.

Motivated by the above considerations, here we anchor fluorescent cholesterol-modified DNA probes (i.e., F-miRNA probe) on dye-loaded QSs, to produce FRET-active nanovesicles responsive to clinically relevant nucleic acid targets such as microRNAs (miRNA), a class of small endogenous non-coding RNAs that can be used as diagnostic and prognostic markers in multiple human diseases.[36–38] Considering that FRET typically occurs within a distance of 1–10 nm, the hybridization of specific sequences to DNA-grafted QSs may produce ratiometric FRET change to be used for miRNA detection. (**Scheme 1**). We demonstrate the versatility and robustness of this approach by functionalizing three types of dye-loaded QSs composed of different surfactants. We experimentally investigated photophysical properties of DNA-grafted FRET QSs and their responsiveness to miRNA targets.

2. Results and Discussion

2.1. Preparation of Fluorescent DNA-Grafted Nanovesicles

We designed three types of fluorescent QS nanovesicles, loaded with 1′-dioctadecyl-3,3,3′3′-tetramethylindocarbocyanine perchlorate (DiI) (here named QS/DiI) prepared by a one-step method using the green technology referred to as depressurization of expanded liquid organic solution–suspension (DELOS-suspension) methodology.[39] To tune the overall surface charge of the fluorescent nanovesicles, we employed either cationic or anionic surfactants, at an equimolar ratio with cholesterol (Chol). The 1:1 bimolecular pair formed by one surfactant and one cholesterol molecule in the following is termed "synthon", since it represents the building block from which the vesicles are formed. In particular, tetradecyldimethylbenzylammonium chloride (MKC) has been employed as cationic surfactant to
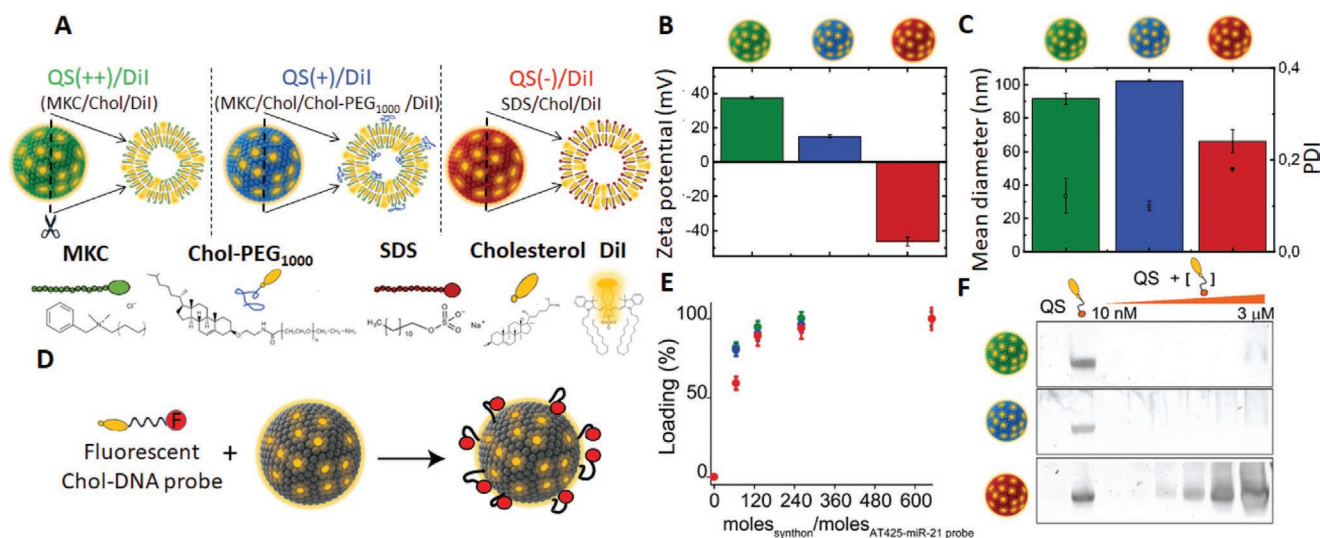
Figure 1. Design and characterization of DNA-functionalized QSs with different composition and surface charge. A) Schematic representation of QSs loaded with the organic dye (DiI). From left to right, QS nanovesicles formed by the self-assembly in water of cholesterol, MKC and DiI (QS(++)/DiI, green particle); cholesterol, MKC, chol-PEG$_{1000}$ and DiI (QS(+)/DiI, blue particle); cholesterol, SDS and DiI (QS(−)/DiI, red particle). B) Zeta-potential analysis of QS(++)/DiI (green), QS(+)/DiI (blue), QS(−)/DiI (red). C) Mean hydrodynamic diameter and polydispersity index (PDI) of the three QS systems measured by DLS. D) Schematic representation of the functionalization of DiI-loaded QS nanovesicles (QS/DiI) with a fluorescent 5′-end cholesteryl-TEG modified DNA probe (i.e., AT425-miR-21 probe). E) AT425-miR-21 probe loading on QS nanovesicles determined from fluorescence quenching assays. F) AT425-miR-21 probe loading on QS nanovesicles estimated from polyacrylamide gel electrophoresis, comparing electrophoretic mobilities at different ratios of synthon/nucleic acid probe, using a fixed concentration of synthon (130 μM) and increasing concentration of probe. All experiments are performed in PBS buffer (94 mM NaCl, 3.1 mM Na$_2$HPO$_4$, 0.9 mM NaH$_2$PO$_4$, pH = 7.4) at 25 °C. The experimental values represent averages of three separate measurements and the error bars reflect the standard deviations.

produce Chol/MKC nanovesicles with high positive surface charge (QS(++)/DiI, **Figure 1**A,B, Table S1, Supporting Information, and also Experimental Section for QS production). Introducing Chol-PEG$_{1000}$-OH into the Chol/MKC formulation, we obtained nanovesicles with a reduced positive surface charge (QS(+)/DiI, Figure 1A), evidenced by a zeta-potential reduction from ≈40 to ≈15 mV (Figure 1B and Table S1, Supporting Information). Using the anionic surfactant Sodium Dodecyl Sulfate (SDS) we produced instead Chol/SDS nanovesicles exhibiting negatively charged surfaces (QS(−)/DiI, Figure 1A,B). All three types of particles exhibit a high vesicle-to-vesicle homogeneity in terms of size, morphology, and unilamellarity, confirmed by dynamic light scattering (DLS) data (Figure 1C and Table S1, Supporting Information) and cryo-transmission electron microscopy (TEM) images (Figure S1, Supporting Information). Of note, no significant variations in size and morphology were observed in dye-containing nanovesicles over time (10 months, Figure S2, Supporting Information), confirming enhanced stability over time compared to the majority of vesicular lipid-based systems and the absence of significant aggregation processes.[30,40]

To generate FRET active systems responsive to nucleic acid targets, we designed fluorescent 5′-end cholesteryl-TEG modified single-stranded DNA probes complementary to different miRNA targets. Specifically, we designed two fluorescent probes fully complementary to miR-21 (ATTO425-labeled miR-21 responsive probe, i.e., AT425-miR-21 probe) and miR-122 (AlexaFluor647-labeled miR-122 responsive probe, i.e., AF647-miR-122 probe), which represent two well-known miRNAs whose level of expression are frequently altered in cancer.[36,37,41–43] Figure 1D shows a scheme of a DNA-functionalized nanovesicle by

insertion of AT425-miR-21 probe. The hydrophobic effect drives the insertion of the cholesterol moiety of AT425-miR-21 probe in the lipophilic core of the bilayer, leading the fluorophore moiety of the probe in close proximity to the dyes embedded in the vesicle surface. To estimate the loading of the amphiphilic fluorescent nucleic acid probe onto the different vesicles we performed quenching assays using a fixed concentration of probe (100 nM) in the presence of QS/DiI nanovesicles (Figure 1E, see Supporting Information for further details). QS(−)/DiI vesicles (red circles) show a lower affinity compared to QS(+)/DiI and QS(++)/DiI, in agreement with the contribution of electrostatic repulsions occurring between negatively charged surface and single-stranded nucleic acid.[44] As expected, the same DNA probe without the cholesteryl-TEG moiety is not able to bind to QS(−)/DiI nanovesicles (Figure S3, Supporting Information). To further demonstrate successful cholesterol-mediated DNA anchoring to QS/DiI nanovesicles, we also performed polyacrylamide gel electrophoresis assays on QSs functionalized with different concentrations of AT425-miR-21probe. As expected, cholesteryl-TEG-modified oligonucleotides interact more efficiently with lipid-based membrane surfaces (Figure 1F and Figure S4, Supporting Information) than nucleic acid probes without the cholesteryl moiety, for all the systems tested.

## 2.2. Photophysical Properties of FRET Active DNA-Grafted QS

The FRET pair of interest is composed of the amphiphilic cyanine dye DiI (1,1″-Dioctadecyl-3,3,3″,3′-tetramethylindocarbocyanine perchlorate, embedded in the QS membrane) and the far-red

fluorophore Alexafluor 647 (conjugated with the nucleic acid probe at the 5′-end), acting as donor and acceptor, respectively. It should be noted that we have also investigated an additional FRET pair, with the DiI fluorophore functioning as acceptor in the QS membrane, and ATTO425 (conjugated to the nucleic acid) as FRET donor. However, the FRET efficiency observed with the ATTO425-DiI pair was significantly lower than using DiI-AlexaFluor647 (Figure S5, Supporting Information). Moreover, the ATTO425-DiI configuration did not provide significant FRET efficiency for all QS formulations (see Figure S5 and S6, Supporting Information, for further information). Thus, in the following, we will focus on QS/DiI nanovesicles functionalized with an Alexafluor 647 (AF647)-labeled miR-122 probe (i.e., AF647-miR-122 probe), as a first model system to demonstrate FRET active QSs responsive to a miRNA target.

Steady-state fluorescence emission of QS/DiI nanovesicles in the absence of AF647-miR-122 probe show identical emission profiles for QS(++)/DiI and QS(+)/DiI, with the characteristic features of DiI emission, with a maximum of emission at ≈565 nm and a shoulder at ≈605 nm (**Figure 2**A, green and blue lines, and Table S2, Supporting Information). The enhanced intensity of the emission band at ≈595 nm combined with the additional shoulder at ≈645 nm in QS(−)/DiI can instead be indicative of aggregation-induced emission phenomena of the cyanine dyes in the lipid nanovesicles (Figure 2A, red line). Absorption and excitation spectra seem to confirm the hypothesis of fluorescent aggregates in QS(−)/DiI nanovesicles (Figures S7 and S8, Supporting Information).[45]

Fluorescence quantum yields (ϕ_F) of DiI embedded in the three QSs (Tables S2 and S3, Supporting Information) confirm

recently reported values.[35] Upon functionalization with AF647-miR-122 probe, fluorescence emission spectra indicate the occurrence of energy transfer in the three QS/DiI systems (Figure 2C). Upon excitation at 520 nm, two bands appear, with maxima at ≈565 and ≈675 nm corresponding to the DiI and AF647 fluorescence emission, respectively. The fluorescence intensity of the donor (DiI) decreases in the presence of the acceptor (AF647), resulting in FRET efficiencies (E_{FRET}) ranging from 80% (QS(+)/DiI/AF647-miR-122 probe) to 25% (QS(−)/DiI/AF647-miR-122 probe, see Table S3, Supporting Information). Excitation spectra obtained when probing acceptor emission at λ_{em} = 750 nm in the presence and in the absence of QS/DiI nanovesicles clearly confirm that changes in fluorescence emission can be ascribed to FRET mechanism in the three systems (Figure 2B and Figure S9, Supporting Information). In addition, a significant red shift of ≈10 nm in the maximum of AF647 emission for QS(++)/DiI/AF647-miR-122 probe (green line) and QS(+)/DiI/AF647-miR-122 probe (blue line) compared to free miR-122 probe (dashed black line) in solution is reported, indicating that positively charged nanovesicles more strongly interact with nucleic acid probes. Of note, FRET efficiency increases as a function of acceptor concentration (AF647), reaching its maximum value in the presence of 200 nM of AF647-miR-122 (Figure S10, Supporting Information). All three nanovesicle systems protect the oligonucleotide probe from nuclease digestion, although to a different extent (Figure S11, Supporting Information), showing no significant degradation when the amphiphilic probe is anchored to highly positively charged QS nanovesicles, and only similar partial degradation when anchored to
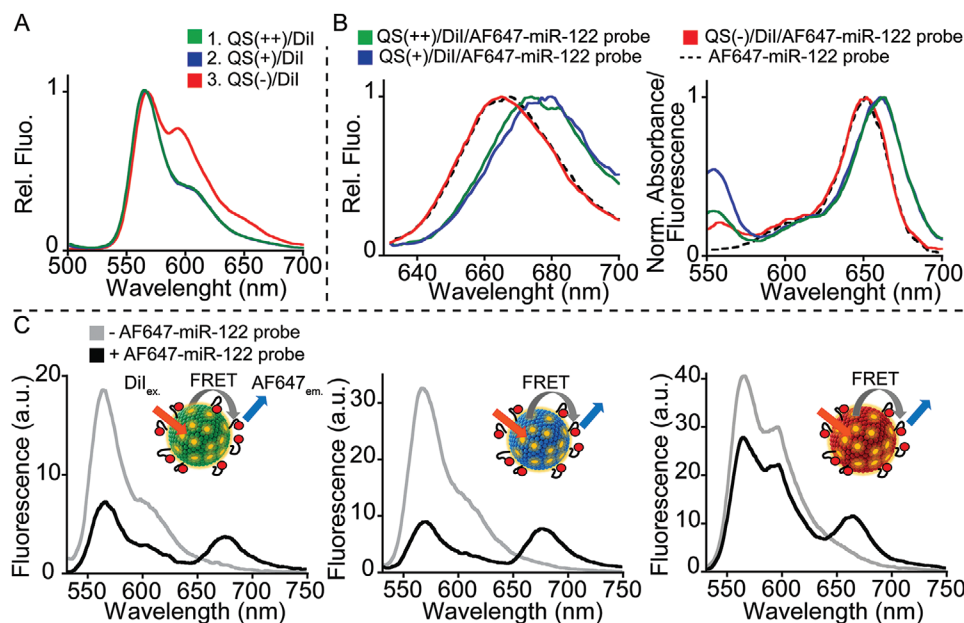
Figure 2. Emission spectra of plain and AF647-miR-122 probe functionalized QS/DiI nanovesicles. A) Normalized emission spectra of QS(++)/DiI (green), QS(+)/DiI (blue), QS(−)/DiI (red) by exciting DiI embedded in the particles (λ_{exc} = 488 nm). B) Normalized emission (left) and excitation fluorescence spectra (right) of QS(++)/DiI/AF647-miR-122 probe (green), QS(+)/DiI/AF647-miR-122 probe (blue), QS(−)/DiI/AF647-miR-122 probe (red) and AF647-miR-122 probe free in solution (dashed black line). Emission spectra are obtained by exciting AF647 at a fixed wavelength (λ_{exc} = 520 nm). Excitation spectra are recorded by fixing the emission at λ_{em} = 750 nm and moving excitation from 550 to 700 nm. C) Emission spectra of QS(++)/DiI (left), QS(+)/DiI (middle), QS(−)/DiI (right) nanovesicles in the absence (grey) and in the presence of AF647-miR-122 probe (200 nM, black line), showing quenching of donor fluorescence (DiI) and increase of acceptor (AF647) emission.

QS(+) and QS(−). This can be ascribed to the high flexibility of single-stranded DNA which can help maximize the electrostatic attraction of negatively charged phosphate backbone to the positively charged vesicle surface, resulting in more flattened configurations of DNA that make the probe inaccessible to nuclease digestion. The similar behavior of QS(+) and QS(−), instead, could be ascribable to the surface charge of QS(+), just slightly positive (≈15 mV) that establishes only weak electrostatic interactions with the negatively charged phosphate backbone, thus not able to completely hinder the nuclease activity of the enzyme towards the DNA probe.

2.3. miRNA Detection using DNA-Grafted QSs

To explore the use of the FRET platform for sensing applications, we tested the possibility of detection of mature miRNAs. We expect the single strand to duplex transition of the miRNA probe to induce a significant probe elongation, resulting in an increase of the average distance between FRET donor and acceptor, and a consequent decrease in FRET efficiency (**Figure 3**A). The hypothesis of a measurable FRET change in the presence of target miRNA relies on the theoretical calculation of the Förster radius (R_0) in the three QS/DiI/AF647-miR-122 probe systems (R_0 is equal to 5.6 ± 0.1 nm, 5.3 ± 0.1 nm, and 5.6 ± 0.1 nm for QS(++), QS(+) and QS(−), respectively, the estimated surface density of acceptor molecules and the expected change in the conformation upon hybridization of target

miRNA (the persistence length of a 22 base long DNA-RNA hybrid is ≈7 nm) (see Supporting Information and Figure S12, Supporting Information).

Ratiometric FRET changes for the three QS/DiI/AF647-miR-122 probe systems are obtained in the presence of complementary target miR-122 (black curves, Figure 3B). Indeed, by adding increasing concentrations of miR-122 we observe an increase in the DiI emission and a consequent decrease of the emission associated with AF647, resulting in a decrease of the FRET efficiencies calculated from the donor's (DiI) steady-state fluorescence (see Table S2, Supporting Information). The three ratiometric detections are quantitative in the nanomolar range of target concentration and highly specific, showing no significant FRET changes in the presence of non-specific target (Figure 3C and Table S4, Supporting Information). More specifically, the target concentrations at which the observed signal change is half the maximum signal change ($K_{1/2}$) are 540 ± 30 nM, 220 ± 10 nM, and 91 ± 9 nM for QS(++), QS(+), and QS(−), respectively. As expected, no specific miRNA target detection is achieved in absence of the hydrophobic cholesterol moiety on the miR-122 probe (Figure S13, Supporting Information), as these probes merely interact electrostatically with the nanovesicle surface and can therefore be displaced from the QS surface at increased concentrations of nucleic acids of arbitrary sequence. To improve the overall sensitivities, we also tested lower concentrations of miR-122 probe anchored on the QS/DiI surface that coherently results in lower limit of detection at the cost of a decrease in the change of ratiometric
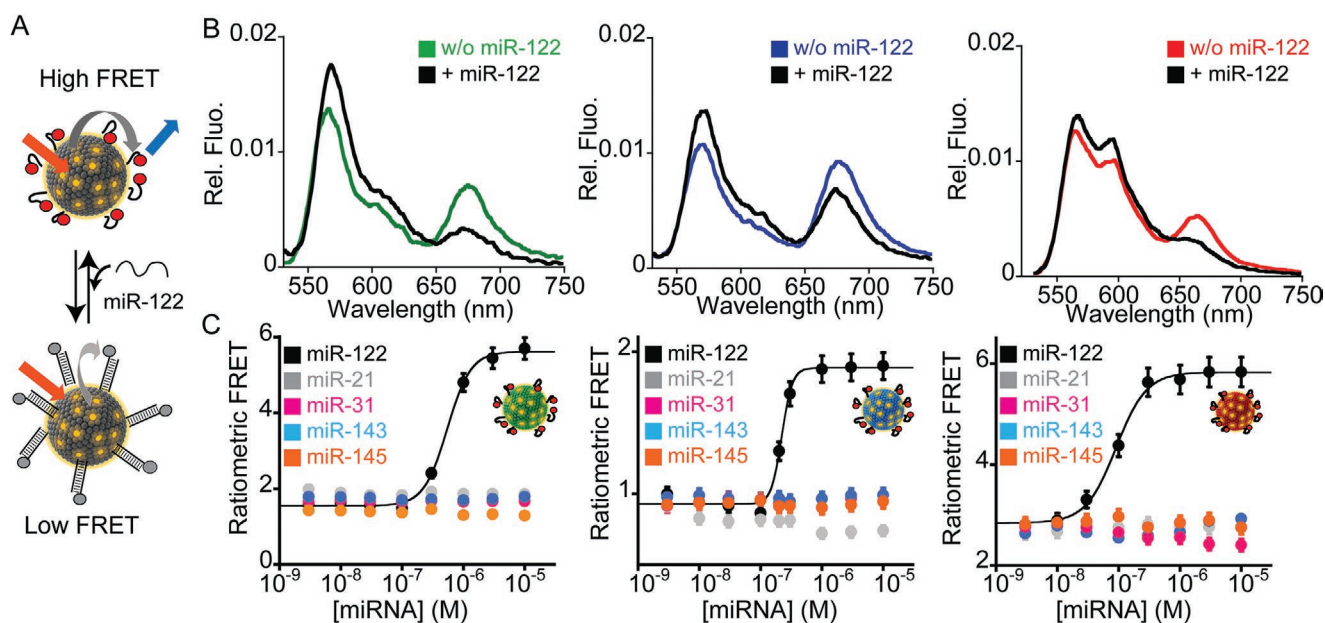
Figure 3. miRNA detection by using FRET-active DNA-grafted QS nanovesicles. A) Schematic representation of the platform for miRNA sensing by using QS/DiI/AF647-miR-122 probe. In the absence of miR-122, AF647-miR-122 probe is anchored on the QS surface in a random coil conformation that allows AF647 (acceptor of the FRET couple) to be in close contact with DiI (donor of the FRET couple) loaded in QS nanovesicle, resulting in a high FRET efficiency. In the presence of the miR-122 target, the binding induces a conformational change of the AF647-miR-122 probe resulting in an increase of the average donor-acceptor distance and lower FRET efficiency. B) Emission spectra of QS(++)/DiI (left), QS(+)/DiI (middle), QS(−)/DiI (right) functionalized with 200 nM of AF647-antimiR-122 probe in the absence (green, blue, and red lines, respectively) and in the presence of miR-122 (i.e., 300 nM, black lines). C) Binding curves obtained by adding increasing concentration of the specific (miR-122, black) or non-specific target (miR-21, grey; miR-31, light blue; miR-143, fuchsia; miR-145, orange) to a solution containing QS/DiI/AF647-miR-122 probe. From left to right the binding curves related to QS(++), QS(+) and QS(−). All the experiments are performed in PBS buffer (94 mM NaCl, 3.1 mM Na₂HPO₄, 0.9 mM NaH₂PO₄, pH 7.4), at 25 °C by exciting vesicle-embedded DiI (λ_{exc} = 520 nm).

FRET (Figure S14, Supporting Information). As expected, by decreasing the concentrations of antimiR-122 from 200 to 30 nM, occupancy is no longer defined by the true affinity of the nucleic acid probe or the concentration of free target in solution but instead by the total number of target molecules in the sample relative to the total number of probes on the sensor surface (i.e., *ligand-depletion* conditions).[46]

3. Conclusions

In this work, we developed and characterized a new platform based on highly stable and bright FRET-active nanovesicles that are responsive to clinically relevant nucleic acid targets. For this purpose, fluorescent amphiphilic nucleic acid probes were anchored on dye-loaded QS nanovesicles through a cholesterol moiety. We demonstrate the specific and ratiometric detection of miRNA with different QS systems, exhibiting either positive or negative surface charges or a functionalization with polyethylene glycol. The possibility to load QS nanovesicles with different donor/acceptor fluorescent pairs and different probes might also allow to achieve multiplex simultaneous detection of molecular targets in an orthogonal way. Indeed, the proposed strategy could be easily adapted to the detection of different biomarkers, by simply using rationally designed amphiphilic structure-switching DNA probes. Although, the overall sensitivity of the platform is still not high enough for clinical monitoring of miRNA levels in vitro, further engineering of both the QS nanovesicle and DNA probe will allow to improve the signal transduction and the overall sensitivity. We also expect to achieve a bioimaging platform for the detection of a wide range of nucleic acids and other clinically relevant molecules (using aptamers) in complex body fluids or directly in cells, thanks to the capability of DNA-grafted QSs for intracellular delivery (Figures S15 and S16, Supporting Information). Besides the sensing applications, the functionalization of lipid vesicles with amphiphilic nucleic acids can provide a means to rationally introduce responsiveness to environmental cues into artificial lipid-based protocells, which represents one of the main challenges in synthetic biology and biomimetic biotechnology. This approach can thus open horizons in the field of multi-functional hybrid nanovesicles for cell imaging and theranostics, since the incorporation of functional amphiphilic probes can be used to improve the targeting ability and help increase the efficacy of therapeutic applications.

4. Experimental Section

Reagents and Materials: Sodium chloride (NaCl), sodium dihydrogen phosphate (NaH$_2$PO$_4$), disodium hydrogen phosphate (Na$_2$HPO$_4$), magnesium chloride (MgCl$_2$), 2-amino-2-(hydroxymethyl)-1,3-propanediol (Tris base), boric acid, ethylenedinitrilo)tetraacetic acid (EDTA), acrylamide/bis-acrylamide 30% solution, ammonium persulfate (APS), *N,N,N′,N′*-tetramethyl ethylenediamine (TEMED), tetradecyldimethylbenzylammonium chloride (MKC), cholesteryl-polyethylene glycol 1000 (Chol-PEG$_{1000}$) were purchased from Sigma-Aldrich, Italy and used without any further purifications. Orange DNA Loading Dye (6×) and O'Range Ruler 5 base pair DNA Ladder were purchased from Thermo Fisher Scientific Italia. 5-Cholesten-3β-ol (Chol, purity 95%) was purchased from Panreac (Barcelona, Spain).

1,1′-dioctadecyl-3,3,3′,3′-tetramethyl-indocarbocyanine perchlorate (DiI) were purchased from Life Technologies (Carlsbad, USA).

Oligonucleotides: Oligonucleotides (HPLC purified) were purchased from Biosearch Technologies (Risskov, Denmark). All oligonucleotides were dissolved in phosphate buffer (1 M NaCl/ 50 mM NaH$_2$PO$_4$, pH = 7) at a concentration of 100 µM and stored at −20 °C. The concentration of the oligonucleotides was confirmed using Tecan Infinite M200pro (Männedorf, Switzerland) through NanoQuant Plate. Fluorescent miRNA probes were terminally modified with a cholesteryl-triethylene glycol (TEG) moiety at 5′-end.

The sequences and modification schemes of the oligonucleotide sequences were as follows:

F-miRNA probes:
AF647-miR-122 probe
5′-Cholesteryl – TEG – CAAACACCA TTGTCACACTCCA – Alexa647-3′
AT425-miR-21 probe
5′-Cholesteryl – TEG – TCA ACA TCA GTC TGA TAA GCT A- ATTO425-3′
Nuclease assays were performed using a miR-122 probe internally labeled with a FRET pair (ATTO425/ATTO550).
miR-21 probe dual labeled
5′-Cholesteryl – TEG – ATTO550- TCA ACA TCA GTC TGA TAA GCT A- ATTO425-3′
To evaluate the effect of cholesterol as anchor for binding to lipid layer, the authors also decorated QS nanovesicles with ATTO425-modified miR-21 probe without cholesterol.
AT425-miR-21 probe w/o chol.
5′- TCA ACA TCA GTC TGA TAA GCT A- ATTO425-3′
miRNA Targets:
miR-122: 5′ – UGG AGU GUG ACA AUG GUG UUUG – 3′
miR-21: 5′- UAG CUU AUC AGA CUG AUG UUGA -3′
miR-31: 5′-AGGCAAGAUGCUGGCAUAGCU-3′
miR-143: 5′-UGAGAUGAAGCACUGUAGCUC-3′
miR-145: 5′-GUCCAGUUUUCCCAGGAAUCCCU-3′
Synthesis of Dye-Loaded QSs: Three different QS vesicles were prepared and tested by using DELOS-SUSP technology:[39]

1) MKC/Chol/DiI (48.5:48.5:1).
2) MKC/Chol/CholPEG$_{1000}$/DiI (48.5:41.5:7:1).
3) SDS/Chol/DiI (48.5:48.5: 1).

The final concentration of synthon is 1.3 mM for all the types of QSs. The concentration of DiI loaded was determined through absorption spectra (see absorption experiments and Table S1, Supporting Information). QS vesicles without embedded DiI were also prepared using the same experimental procedure in the absence of dye.

Preparation of FRET Active DNA-Grafted QSs: Thanks to the ability of cholesterol to act as anchor for the lipid layer, FRET active DNA-grafted QSs were prepared by simply mixing QS/DiI and F-miRNA probe terminally modified with cholesteryl-TEG moiety, in PBS buffer (94 mM NaCl, 3.1 mM Na$_2$HPO$_4$, 0.9 mM NaH$_2$PO$_4$, pH 7.4) and waiting 10 min to allow cholesterol insertion on the nanovesicle.

Fluorescence Assays: All fluorescence measurements were performed in 45 µL solution of Na$_2$HPO$_4$ (3.1 mM) + NaH$_2$PO$_4$ (0.9 mM) + NaCl (94 mM) at pH 7.4 at 25 °C. Steady state fluorescence measurements were obtained using a Cary Eclipse Fluorimeter. In the experiments performed using AT425-miR-21 probe (AT425 acting as FRET donor), emission spectra was recorded with excitation at 420 nm and acquisition from 430 to 750 nm. Excitation spectra was recorded with emission at 700 nm and acquisition from 360 to 650 nm. In the experiments performed using AF647-miR-122 probe (AF647 acts as FRET acceptor), emission was recorded spectra with excitation at 520 nm and acquisition from 540 to 750 nm. Excitation spectra was recorded with emission at 750 nm and acquisition from 550 to 700 nm. The excitation and emission bandwidths were fixed to 5 nm in all the experiments. The binding curves reported in Figure 3C and Figure S14, Supporting Information, were obtained by sequentially increasing the concentration of miRNA target to a solution containing a fixed concentration of the synthon (26 µM) and AF647-miR-122 probe (200 nM) and taking in account the relative increase of the volume. DNA loading fluorescence experiments were

performed (reported Figures 2E and Figure S3, Supporting Information), by adding increasing concentrations of synthon to a solution containing fixed amount of AT425-miR-21 probe (100 nM). Nuclease experiments were performed by adding 10 µg of DNAse I in 45 µL of solution containing 30 nM of miR-21 probe dual labeled with and without QS nanovesicles (synthon equal to 26 µM). Kinetic curves were performed with excitation at 445 nm and acquisition at 480 nm, bandwidths of 5 nm in excitation and emission.

Absorption Experiments: All the absorbance measurements were performed in 100 µL solution of Na_2HPO_4 (3.1 mM) + NaH_2PO_4 (0.9 mM) + NaCl (94 mM) at pH 7.4 at 25 °C, using cuvette Hellma quartz cells (1 cm pathlength) and a Varian Cary 50 UV–Vis Spectrophotometer. To determine the concentration of DiI entrapped in the QS particles, the UV–Vis absorbance of the dye was measured by diluting the samples in ethanol, in order to dissociate QS membranes, until an absorbance value of 0.1–0.3 was obtained. The concentration of the dye was determined using Lambert–Beer law ($\varepsilon_{550\,nm}^{DiI}$ in EtOH = 140 000 M^{-1} cm^{-1}).[47]

Native Polyacrylamide Gel Electrophoresis (PAGE) Assays: Native PAGE experiments were performed by using 12% polyacrylamide (29:1 acrylamide/bisacrylamide) in TBE 10× buffer (1 M Tris, 0.9 M boric acid, and 0.01 M EDTA), pH 8.3. The gel solution was prepared by mixing 5.7 mL of diH$_2$O, 4.1 mL of TBE 10× buffer, 4.2 mL of 30% acrylamide/bisacrylamide solution, 75 µL of 10% APS, 14 µL of TEMED. A volume of 20 µL of each sample was mixed with 1 µL of Orange DNA Loading Dye (6×) and then the mixture was added into the gel for the electrophoresis. O'Range Ruler 5 base pair DNA Ladder was used as the DNA standard. The native PAGE was carried out in a Mini-PROTEAN Tetra cell electrophoresis unit (Bio-Rad) at room temperature, at a constant voltage of 90 V, using TBE 1× buffer (0.1 M Tris, 0.09 M boric acid, and 0.001 M EDTA) at pH 8.3 for 3 h. After 30 min of staining in SYBR gold (Invitrogen) dissolved in a TBE 1× buffer at pH 8.3, the gel was scanned by a Gel Doc XR+ system (Bio-Rad).

Cryogenic Transmission Electronic Microscopy: Cryogenic transmission electronic microscopy (cryoTEM) images was acquired with a JEOL JEM microscope (JEOL JEM 2011, Tokyo, Japan) operating at 200 kV under low-dose conditions. The sample was deposited onto the holey carbon grid and then it was immediately vitrified by rapid immersion in liquid ethane. The vitrified sample was mounted on a cryo-transfer system (Gatan 626) and it was introduced into the microscope. Images were recorded on a CCD camera (Gatan Ultrascan US1000) and they were analyzed with the Digital Micrograph 1.8 software.

Dynamic Light Scattering (DLS): The authors measured the size, polydispersity index and ζ-Potential of all the nanovesicles produced using a Zetasizer Nano ZS (Malvern Instruments) with an incident light of 633 nm and measuring the scattered light at 173°. A DTS1070 folded capillary cell (Malvern Instruments) was used to perform ζ-Potential measurements, applying a voltage of 20 mV between the electrodes. The measurements was performed without dilution at 298 K and Smoluchowski equation was employed. To ensure the reliability of the results, three different experiments was performed for each sample.

Loading of miRNA Probe on QS Surface (%): For each concentration of QS nanovesicles, loading was estimated as follows

$$Loading(\%) = \frac{F_{(QS/DiI/AT425\text{-}miR\text{-}21probe)} - F_{(AT425\text{-}miR\text{-}21probe)}}{F_{(max)} - F_{(AT425\text{-}miR\text{-}21probe)}} \times 100 \quad (1)$$

where $F_{(QS/DiI/AT425\text{-}miRNA\,probe)}$) is the fluorescence signal of AT425-miR-21 probe at the maximum ($\lambda_{em\,max}$ = 485 nm) in the presence of QS/DiI nanovesicles and $F_{(AT425\text{-}miRNA\,probe)}$) is the fluorescence signal of AT425-miR-21 probe in the absence of QS nanovesicles.

Binding Curve Analysis: Ratiometric FRET values were calculated as follows

$$Rat.FRET = \frac{Fluorescence_{(Donor)}}{Fluorescence_{(Acceptor)}} \quad (2)$$

The binding curves reported in Figures 3C and Figure S14, Supporting Information, were fitted with the following four parameter logistic equation:

$$Rat.FRET(T) = Rat.FRET_0 + (Rat.FRET_B - Rat.FRET_0) \times \frac{[T]^{nH}}{[T]^{nH} + K_{1/2}^{nH}} \quad (3)$$

where Rat. FRET (T) is the FRET value in the presence of different concentration of target; Rat. $FRET_0$ = ratiometric FRET value in the absence of target; [T] = target concentration; Rat. $FRET_B$ = ratiometric FRET in the presence of saturating concentration of target; $K_{1/2}$ = the observed equilibrium concentration at half-maximum signal gain; n_H = the Hill coefficient.

Determination of Fluorophore Quantum Yield: The fluorescence quantum yield (ϕF) of DiI comparatively was determined,[48] using rhodamine 6G in ethanol as standard.[49]

The values were calculated according to the following equation:

$$\varphi = \varphi(standard) \cdot \frac{F(DiI)}{F(standard)} \cdot \frac{Abs(standard)}{Abs(DiI)} \cdot \left(\frac{n_{(DiI)}}{n_{(standard)}}\right)^2 \quad (4)$$

where $\varphi(standard)$ is the quantum yield of the rhodamine 6G in ethanol (0.94);[49] F(DiI) and F(standard) were the total fluorescence emission values of DiI and rhodamine 6G (between 500 and 710 nm), respectively, by exciting the samples at 488 nm; Abs(DiI) and Abs(standard) were the absorbance values at 488 nm of DiI and rhodamine 6G; and n indicates the refractive index of the solvent in the two sample.

FRET Efficiency and Förster Radius: FRET efficiencies were calculated from the decrease in donor's (DiI) steady state fluorescence, by using the following equation

$$E = 1 - \frac{F_A}{F_0} \quad (5)$$

where F_A and F_0 are the fluorescence emission values of DiI at 567 nm, in the presence and in the absence of the acceptor AF647, respectively.

Förster radii were calculated for the three different QS samples using the following equation:

$$R_0^6 = 8.785 * 10^{-5} \frac{\frac{2}{3} \varphi_D J}{n^4} \quad (6)$$

where φ_D is the quantum yield of the donor, in the absence of the acceptor, n is the refractive index of the medium (water, 1.333), and J is the spectral overlap integral calculated as

$$J = \int F_D(\lambda) \varepsilon_A(\lambda) \lambda^4 d\lambda \quad (7)$$

where F_D is the donor (QS/DiI) emission spectrum normalized to an area of 1, and ε_A is the acceptor (AF647) molar extinction coefficient (expressed as M^{-1} cm^{-1}) and the wavelength is expressed in nm.

Cell Lines: HEK293T were purchased from American Type Culture Collection (ATCC, Manassas, VA, USA) and stored in liquid nitrogen. Upon resuscitation, HEK293T cells were cultured in Dulbecco's Modified Eagle Medium (DMEM) (Life Technologies, Thermo Fisher Scientific, Waltham, Massachusetts, USA), supplemented with 10% heat-inactivated fetal bovine serum (FBS) South America Premium (Thermo Fisher Scientific), 100 U mL^{-1} penicillin, 100 µg mL^{-1} streptomycin (Thermo Fisher Scientific) and 5 µg mL^{-1} plasmocin (InvivoGen, San Diego, CA, USA). All cultures were maintained at 37 °C in a saturated atmosphere of 95% air and 5% CO2. HEK293T cells were tested for mycoplasma contamination periodically.

**ADVANCED
SCIENCE NEWS**

www.advancedsciencenews.com

**ADVANCED
FUNCTIONAL
MATERIALS**

www.afm-journal.de

Confocal Imaging: HEK293T cells were seeded at 5.5×10^4 in 8-wells Ibidi chamber slides coated with poly-L-lysine (#80 824; Ibidi) in DMEM supplemented with 10% FBS without antibiotics. DNA-grafted QS were prepared by the combination of 10 µg mL^{-1} QS(+) and 50 nM of dual labeled miR-21 probe or 10 µg mL^{-1} QS (+)/DiI and 50 nM of AF647-miR-122 probe labeled with Alexa647 and incubated with HEK293T cells for 24 h. The next day, cellular media was changed and images of five random fields were acquired using a Leica TCS SP8 microscope equipped with a white light laser and Hybrid spectral detectors (Leica Microsystems GmbH, Mannheim, Germany). The confocal images were performed using a HC x PL APO 63×/1.4 oil immersion objective and module resonant scanner. ATTO425 was excited with a blue diode laser (blue channel, 405 nm) and detected in the 420–520 nm. ATTO550 and DiI were excited with a white light laser (green channel, 558 nm) and detected in the 565–635 nm. Lysosomes were stained with Lysotracker Deep Red (1:1000 from stock 1 mM) (#L12492; Thermo Fisher Scientific), excited with a white light laser (red channel, 645 nm) and detected in the 660–795 nm. QS fluorescence and transmitted light imaging were combined to study the DNA-grafted QSs distribution inside the cell. One Z-section was acquired using a pinhole of 0.8 Airy unit and images were processed using the ImageJ Fiji software (National Institutes of Health, Bethesda, MD, USA).

Supporting Information

Supporting Information is available from the Wiley Online Library or from the author.

Conflict of Interest

The authors declare no conflict of interest.

Data Availability Statement

Research data are not shared.

[1] N. P. Kamat, J. S. Katz, D. A. Hammer, *J. Phys. Chem. Lett.* **2011**, *2*, 1612.

[2] I. A. Chen, P. Walde, *Cold Spring Harbor Perspect. Biol.* **2010**, *2*, a002170.

[3] A. M. Carmona-Ribeiro, *Chem. Soc. Rev.* **1992**, *21*, 209.

[4] E. Rideau, R. Dimova, P. Schwille, F. R. Wurm, K. Landfester, *Chem. Soc. Rev.* **2018**, *47*, 8572.

[5] A. Puri, K. Loomis, B. Smith, J.-H. Lee, A. Yavlovich, E. Heldman, R. Blumenthal, *Crit. Rev. Ther. Drug Carrier Syst.* **2009**, *26*, 523.

[6] P. A. Beales, T. K. Vanderlick, *Adv. Colloid Interface Sci.* **2014**, *207*, 290.

[7] L. Parolini, B. M. Mognetti, J. Kotar, E. Eiser, P. Cicuta, L. Di Michele, *Nat. Commun.* **2015**, *6*, 5948.

[8] L. Parolini, J. Kotar, L. Di Michele, B. M. Mognetti, *ACS Nano* **2016**, *10*, 2392.

[9] J. Liu, V. Postupalenko, S. Lörcher, D. Wu, M. Chami, W. Meier, C. G. Palivan, *Nano Lett.* **2016**, *16*, 7128.

[10] K. Göpfrich, T. Zettl, A. E. C. Meijering, S. Hernández-Ainsa, S. Kocabey, T. Liedl, U. F. Keyser, *Nano Lett.* **2015**, *15*, 3134.

[11] U. F. Keyser, *Nat. Nanotechnol.* **2016**, *11*, 106.

[12] P. Chidchob, D. Offenbartl-Stiegert, D. McCarthy, X. Luo, J. Li, S. Howorka, H. F. Sleiman, *J. Am. Chem. Soc.* **2019**, *141*, 1100.

[13] X. Li, K. Feng, L. Li, L. Yang, X. Pan, H. S. Yazd, C. Cui, J. Li, L. Moroz, Y. Sun, B. Wang, X. Li, T. Huang, W. Tan, *Natl. Sci. Rev.* **2020**, *7*, 933.

[14] M. You, Y. Lyu, D. Han, L. Qiu, Q. Liu, T. Chen, C. S. Wu, L. Peng, L. Zhang, G. Bao, W. Tan, *Nat. Nanotechnol.* **2017**, *12*, 453.

[15] I. Insua, J. Montenegro, *Chem* **2020**, *6*, 1652.

[16] Y. Lyu, R. Peng, H. Liu, H. Kuai, L. Mo, D. Han, J. Li, W. Tan, *Chem. Sci.* **2020**, *11*, 631.

[17] A. Joesaar, S. Yang, B. Bögels, A. van der Linden, P. Pieters, B. V. V. S. P. Kumar, N. Dalchau, A. Phillips, S. Mann, T. F. A. de Greef, *Nat. Nanotechnol.* **2019**, *14*, 369.

[18] A. Rodríguez-Pulido, A. I. Kondrachuk, D. K. Prusty, J. Gao, M. A. Loi, A. Herrmann, *Angew. Chem., Int. Ed.* **2013**, *52*, 1008.

[19] V. Allain, C. Bourgaux, P. Couvreur, *Nucleic Acids Res.* **2012**, *40*, 1891.

[20] R. Lanfranco, P. K. Jana, G. Bruylants, P. Cicuta, B. M. Mognetti, L. Di Michele, *Nanoscale* **2020**, *12*, 18616.

[21] J. Liu, I. Craciun, A. Belluati, D. Wu, S. Sieber, T. Einfalt, D. Witzigmann, M. Chami, J. Huwyler, C. G. Palivan, *Nanoscale* **2020**, *12*, 9786.

[22] P. M. G. Löffler, O. Ries, A. Rabe, A. H. Okholm, R. P. Thomsen, J. Kjems, S. Vogel, *Angew. Chem., Int. Ed.* **2017**, *56*, 13228.

[23] J. A. Peruzzi, M. L. Jacobs, T. Q. Vu, K. S. Wang, N. P. Kamat, *Angew. Chem., Int. Ed.* **2019**, *58*, 18683.

[24] S. J. Bachmann, J. Kotar, L. Parolini, A. Šarić, P. Cicuta, L. Di Michele, B. M. Mognetti, *Soft Matter* **2016**, *12*, 7804.

[25] U. Kauscher, M. N. Holme, M. Björnmalm, M. M. Stevens, *Adv. Drug Delivery Rev.* **2019**, *138*, 259.

[26] Z. Al-Ahmady, K. Kostarelos, *Chem. Rev.* **2016**, *116*, 3883.

[27] C. B. Minkenberg, F. Li, P. van Rijn, L. Florusse, J. Boekhoven, M. C. A. Stuart, G. J. M. Koper, R. Eelkema, J. H. van Esch, *Angew. Chem., Int. Ed.* **2011**, *50*, 3421.

[28] S. F. Shimobayashi, B. M. Mognetti, L. Parolini, D. Orsi, P. Cicuta, L. Di Michele, *Phys. Chem. Chem. Phys.* **2015**, *17*, 15615.

[29] L. Ferrer-Tasies, E. Moreno-Calvo, M. Cano-Sarabia, M. Aguilella-Arzo, A. Angelova, S. Lesieur, S. Ricart, J. Faraudo, N. Ventosa, J. Veciana, *Langmuir* **2013**, *29*, 6519.

[30] N. Grimaldi, F. Andrade, N. Segovia, L. Ferrer-Tasies, S. Sala, J. Veciana, N. Ventosa, *Chem. Soc. Rev.* **2016**, *45*, 6520.

[31] G. Vargas-Nadal, M. Muñoz-Ubeda, P. Alamo, M. M. Arnal, V. Céspedes, M. Köber, E. Gonzalez, L. Ferrer-Tasies, M. P. Vinardell, R. Mangues, J. Veciana, N. Ventosa, *Nanomedicine* **2020**, *24*, 102136.

[32] X. Liu, A. Ardizzone, B. Sui, M. Anzola, N. Ventosa, T. Liu, J. Veciana, K. D. Belfield, *ACS Omega* **2017**, *2*, 4112.

[33] A. Ardizzone, D. Blasi, D. Vona, A. Rosspeintner, A. Punzi, E. Altamura, N. Grimaldi, S. Sala, E. Vauthey, G. M. Farinola, I. Ratera, N. Ventosa, J. Veciana, *Chem. - Eur. J.* **2018**, *24*, 11386.

[34] A. Ardizzone, S. Kurhuzenkau, S. Illa-Tuset, J. Faraudo, M. Bondar, D. Hagan, E. W. Van Stryland, A. Painelli, C. Sissa, N. Feiner, L. Albertazzi, J. Veciana, N. Ventosa, *Small* **2018**, *14*, 1703851.

[35] J. Morla-Folch, G. Vargas-Nadal, T. Zhao, C. Sissa, A. Ardizzone, S. Kurhuzenkau, M. Köber, M. Uddin, A. Painelli, J. Veciana, K. D. Belfield, N. Ventosa, *ACS Appl. Mater. Interfaces* **2020**, *12*, 20253.

[36] C. L. Au Yeung, N. N. Co, T. Tsuruga, T. L. Yeung, S. Y. Kwan, C. S. Leung, Y. Li, E. S. Lu, K. Kwan, K. K. Wong, R. Schmandt, K. H. Lu, S. C. Mok, *Nat. Commun.* **2016**, *7*, 11150.

[37] J. D. Campbell, A. Alexandrov, J. Kim, J. Wala, A. H. Berger, C. S. Pedamallu, S. A. Shukla, G. Guo, A. N. Brooks, B. A. Murray, M. Imielinski, X. Hu, S. Ling, R. Akbani, M. Rosenberg, C. Cibulskis, A. Ramachandran, E. A. Collisson, D. J. Kwiatkowski, M. S. Lawrence, J. N. Weinstein, R. G. W. Verhaak, C. J. Wu, P. S. Hammerman, A. D. Cherniack, G. Getz, M. N. Artyomov, R. Schreiber, R. Govindan, M. Meyerson, *Nat. Genet.* **2016**, *48*, 607.

[38] R. Rupaimoole, F. J. Slack, *Nat. Rev. Drug Discovery* **2017**, *16*, 203.

[39] I. Cabrera, E. Elizondo, O. Esteban, J. L. Corchero, M. Melgarejo, D. Pulido, A. Córdoba, E. Moreno, U. Unzueta, E. Vazquez, I. Abasolo, S. Schwartz, A. Villaverde, F. Albericio, M. Royo, M. F. García-Parajo, N. Ventosa, J. Veciana, *Nano Lett.* **2013**, *13*, 3766.

[40] M. Antonietti, S. Förster, *Adv. Mater.* **2003**, *15*, 1323.

[41] C. J. Creighton, M. Morgan, P. H. Gunaratne, D. A. Wheeler, R. A. Gibbs, G. Robertson, A. Chu, R. Beroukhim, K. Cibulskis, S. Signoretti, F. Vandin, H. T. Wu, B. J. Raphael, R. G. W. Verhaak, P. Tamboli, W. Torres-Garcia, R. Akbani, J. N. Weinstein, V. Reuter, J. J. Hsieh, A. R. Brannon, A. A. Hakimi, A. Jacobsen, G. Ciriello, B. Reva, C. J. Ricketts, W. M. Linehan, J. M. Stuart, W. K. Rathmell, S. Hui, P. W. Laird, D. Muzny, C. Davis, X. Liu, K. Chang, N. Kakkar, L. R. Treviño, S. Benton, J. G. Reid, D. Morton, H. Doddapaneni, H. Yi, L. Lewis, D. Huyen, C. Kovar, Y. Zhu, J. Santibanez, W. Min, W. Hale, D. Kalra, G. Getz, M. S. Lawrence, C. Sougnez, S. L. Carter, A. Sivachenko, L. Lee, C. Stewart, D. Voet, S. Fisher, S. B. Gabriel, E. Lander, S. E. Schumacher, B. Tabak, G. Saksena, R. C. Onofrio, A. D. Cherniack, J. Gentry, K. Ardlie, M. Meyerson, H. J. E. Chun, A. J. Mungall, P. Sipahimalani, D. Stoll, A. Ally, M. Balasundaram, Y. S. N. Butterfield, R. Carlsen, C. Carter, E. Chuah, R. J. N. Coope, N. Dhalla, S. Gorski, R. Guin, C. Hirst, M. Hirst, R. A. Holt, C. Lebovitz, D. Lee, H. I. Li, M. Mayo, R. A. Moore, E. Pleasance, P. Plettner, J. E. Schein, A. Shafiei, J. R. Slobodan, A. Tam, N. Thiessen, R. J. Varhol, N. Wye, Y. Zhao, I. Birol, S. J. M. Jones, M. A. Marra, J. T. Auman, D. Tan, C. D. Jones, K. A. Hoadley, P. A. Mieczkowski, L. E. Mose, S. R. Jefferys, M. D. Topal, C. Liquori, Y. J. Turman, S. Yan, S. Waring, E. Buda, J. Walsh, J. Wu, T. Bodenheimer, A. P. Hoyle, J. V. Simons, M. G. Soloway, S. Balu, J. S. Parker, D. N. Hayes, C. M. Perou, R. Kucherlapati, P. Park, T. Triche, D. J. Weisenberger, P. H. Lai, M. S. Bootwalla, D. T. Maglinte, S. Mahurkar, B. P. Berman, D. J. Van Den Berg, L. Cope, S. B. Baylin, M. S. Noble, D. DiCara, H. Zhang, J. Cho, D. I. Heiman, N. Gehlenborg, W. Mallard, L. Pei, S. Frazer, P. Stojanov, Y. Liu, L. Zhou, J. Kim, L. Chin, C. Benz, C. Yau, S. M. Reynolds, I. Shmulevich, R. Vegesna, H. Kim, Z. Wei, D. Cogdell, E. Jonasch, Z. Ding, Y. Lu, N. Zhang, A. K. Unruh, T. D. Casasent, C. Wakefield, D. Tsavachidou, G. B. Mills, J. Gao, E. Cerami, B. Gross, B. A. Aksoy, R. Sinha, N. Weinhold, S. O. Sumer, B. S. Taylor, R. Shen, I. Ostrovnaya, M. F. Berger, M. Ladanyi, C. Sander, S. S. Fei, A. Stout, P. T. Spellman, D. L. Rubin, T. T. Liu, N. Sam, E. O. Paull, D. Carlin, T. Goldstein, P. Waltman, K. Ellrott, Z. Jing, D. Haussler, W. Xiao, C. Shelton, J. Gardner, R. Penny, M. Sherman, D. Mallery, S. Morris, J. Paulauskis, K. Burnett, T. Shelton, W. G. Kaelin, T. Choueiri, M. B. Atkins, E. Curley, S. Tickoo, L. Thorne, L. Boice, H. Mei, J. C. Fisher, C. D. Vocke, J. Peterson, R. Worrell, M. J. Merino, L. S. Schmidt, B. A. Czerniak, K. D. Aldape, C. G. Wood, J. Boyd, J. E. Weaver, M. V. Iacocca, N. Petrelli, G. Witkin, J. Brown, C. Czerwinski, L. Huelsenbeck-Dill, B. Rabeno, J. Myers, C. Morrison, J. Bergsten, J. Eckman, J. Harr, C. Smith, K. Tucker, L. A. Zach, W. Bshara, C. Gaudioso, R. Dhir, J. Maranchie, J. Nelson, A. Parwani, C. O. Potapova, K. Fedosenko, J. C. Cheville, R. H. Thompson, J. M. Mosquera, M. A. Rubin, M. L. Blute, T. Pihl, M. Jensen, R. Sfeir, A. Kahn, A. Chu, P. Kothiyal, E. Snyder, J. Pontius, B. Ayala, M. Backus, J. Walton, J. Baboud, D. Berton, M. Nicholls, D. Srinivasan, R. Raman, S. Girshik, P. Kigonya, S. Alonso, R. Sanbhadti, S. Barletta, D. Pot, M. Sheth, J. A. Demchok, T. Davidsen, Z. Wang, L. Yang, R. W. Tarnuzzer, J. Zhang, G. Eley, M. L. Ferguson, K. R. Mills Shaw, M. S. Guyer, B. A. Ozenberger, H. J. Sofia, *Nature* **2013**, *499*, 43.

[42] S.-H. Hsu, B. Wang, J. Kota, J. Yu, S. Costinean, H. Kutay, L. Yu, S. Bai, K. L. Perle, R. R. Chivukula, J. T. Mendell, K. Ghoshal, *J. Clin. Invest.* **2012**, *122*, 2871.

[43] M. Leina, J. Liu, J. Shen, L. Liu, J. Wu, W. Li, J. Luo, Q. Chen, C. Qian, *Cancer Biol. Ther.* **2010**, *9*, 554.

[44] A. Lopez, J. Liu, *Langmuir* **2018**, *34*, 15000.

[45] F. García-Jiménez, M. I. Khramov, R. Sánchez-Obregón, O. Collera, *Chem. Phys. Lett.* **2000**, *331*, 42.

[46] F. Ricci, A. Vallée-Bélisle, A. J. Simon, A. Porchetta, K. W. Plaxco, *Acc. Chem. Res.* **2016**, *49*, 1884.

[47] A. Mishra, R. K. Behera, P. K. Behera, B. K. Mishra, G. B. Behera, *Chem. Rev.* **2000**, *100*, 1973.

[48] J. R. Lakowicz, *Principles of Fluorescence Spectroscopy*, Springer, Berlin, Germany **2006**.

[49] M. Fischer, J. Georges, *Chem. Phys. Lett.* **1996**, *260*, 115.